IOPscience iopscience.iop.org

Home Search Collections Journals About Contact us My IOPscience

Exchange and crystalline electric fields and magnetization processes in $Pr_2Co_{14}B$ and $Nd_2Co_{14}B$

This article has been downloaded from IOPscience. Please scroll down to see the full text article.

1991 J. Phys.: Condens. Matter 3 195

(http://iopscience.iop.org/0953-8984/3/2/006)

View the table of contents for this issue, or go to the journal homepage for more

Download details:
IP Address: 171.66.16.151
The article was downloaded on 11/05/2010 at 07:03

Please note that terms and conditions apply.

J. Phys.: Condens. Matter 3 (1991) 195–202. Printed in the UK

Exchange and crystalline electric fields and magnetization processes in $Pr_2Co_{14}B$ and $Nd_2Co_{14}B$

Yan Yu, Zhao Tiesong and Jin Hanmin
Department of Physics, Jilin University, Changchun 130023, People's Republic of China

Received 2 May 1990, in final form 17 September 1990

Abstract. The values of R–Co exchange field and crystalline electric field parameters A_{nm} in the compounds $Pr_2Co_{14}B$ and $Nd_2Co_{14}B$ are evaluated by fitting calculations to experiments. The experiments include the magnetization curves along the crystal axes at 4.2 and 290 K and the spin reorientation temperatures for $Pr_2Co_{14}B$ and $Nd_2Co_{14}B$, and also the magnetization curves along the [100] axis at a series of temperatures between 77 and 190 K for $Nd_2Co_{14}B$. A_{nm} is nearly proportional to $\langle r^n \rangle$, and the sign of A_{30} is opposite to that for $R_2Fe_{14}B$. A_{20} decreases smoothly with increase in temperature in a similar way for $Pr_2Co_{14}B$ and $Nd_2Co_{14}B$. The magnetization processes of the rare-earth and the Co sublattices are analysed.

1. Introduction

In recent years the magnetic properties of the compounds $Pr_2Co_{14}B$ and $Nd_2Co_{14}B$ have been studied extensively [1–12]. The easy-magnetization direction (EMD) of $Pr_2Co_{14}B$ is along the c axis below the spin reorientation (SR) temperature $T_{SR} = 664$ K and is in the c plane above T_{SR} [3]. The properties of $Nd_2Co_{14}B$ are more complicated. The EMD is tilted 11–12° away from the c axis at 4.2 K [6, 7]. It approaches the c axis on an increase in temperature and becomes parallel to the c axis at the lower SR temperature $T_{SR} = 37$–38 K [6, 7, 11] and remains in this state up to the higher SR temperature $T_{SR} = 550$ K [10]. Above the higher SR temperature, the EMD lies in the c plane. For this compound, the first-order magnetization process (FOMP) occurs along the [100] axis at lower temperatures [8, 9, 11].

Some workers estimated the values of the exchange field H_{ex} and crystalline-electric-field (CEF) parameters A_{nm} in the compounds by fitting calculations to experiments. Li *et al* [12] obtained the values for $Nd_2Co_{14}B$ from the experiments on the temperature dependence of the spontaneous magnetization $M_s(T)$, the magnetization curves $M(H)$ along the crystal axes at 4.2 K and the SR temperatures. The $M_s(T)$ curve is fitted neglecting the CEF effect, and the fitting of the other experiments was carried out without taking into account the mixing of the excited J multiplets. Kato *et al* [11] evaluated the values of the parameters for $Pr_2Co_{14}B$ from the $M(H)$ curves at 4.2 and 290 K, and for $Nd_2Co_{14}B$ from similar $M(H)$ curves and the lower SR temperature. In their calculation the mixing of the excited J multiplets was taken into account [11]. Our examination, however, shows that the parameters of Kato *et al* fail to reproduce the higher SR temperature for both compounds and the series of $M(H)$ curves along the [100] axis

0953-8984/91/020195 +08 $03.50 © 1991 IOP Publishing Ltd

between 77 and 190 K for the Nd compound. For example, the critical field of FOMP at 90 K is calculated to be 210 kOe compared with the experimental value of 170 kOe [9].

This reveals that it is impossible to reproduce the series of experiments on $Pr_2Co_{14}B$ or $Nd_2Co_{14}B$ by using a set of CEF parameters which are independent of temperature. This paper shows that the experiments can be reproduced well by assuming smooth variations in A_{20} and A_{22} with temperature which are similar for $Pr_2Co_{14}B$ and $Nd_2Co_{14}B$. By using the fitted parameters, the magnetization processes of the rare-earth and the Co sublattices are analysed briefly.

2. Method of calculation

If we neglect the difference between the f and g sites, there are two magnetically inequivalent rare-earth sites: R(1) and R(2). It is assumed that the rare earth is triply ionized. The Hamiltonian of the R(i) ion consists of the CEF, the R–Co exchange, the spin–orbit coupling and Zeeman interactions:

$$\mathcal{H}(i) = \sum_{nm} A_{nm}(i) \left(\frac{4\pi}{(2n+1)}\right)^{1/2} \sum_j Y_{nm}(\theta_j, \varphi_j) - 2\mu_B S \cdot H_{ex} + \lambda S \cdot L + \mu_B (L + 2S) \cdot H \tag{1}$$

where

$$A_{nm}(1) = (-1)^{m/2} A_{n-m}(1) = (-1)^{m/2} A_{nm}(2) \qquad (n = 2, 4, 6; m = 0, \pm 2, \pm 4, \pm 6; |m| \leq n) \tag{2}$$

in the ⟨100⟩ coordinate system with the z axis along the c axis. A_{nm} and H_{ex} are the averages over the f and g sites, and (θ_j, φ_j) are the polar angles of the jth 4f-electron position vector. The matrix elements of $\mathcal{H}(i)$ are calculated by using the irreducible tensor operator technique [13]. For a given H and H_{ex}, the eigenvalues $E_l(i)$ and eigenfunctions $|i, l\rangle$ are obtained by diagonalizing $\mathcal{H}(i)$ within the space consisting of the ground and the first excited J multiplets with $\lambda = 610$ K and 536 K for the Pr and Nd ion, respectively [14]. The free energy of the $R_2Co_{14}B$ system is given by

$$F(H, H_{ex}, T) = -kT \sum_i \ln Z(i) + K_{Co} \sin^2 \theta_{Co} - M_{Co} \cdot H \tag{3}$$

where

$$Z(i) = \sum_l \exp\left(-\frac{E_l(i)}{kT}\right) \qquad \left(l = 1, 2, \ldots, \sum_J (2J+1)\right) \tag{4}$$

and θ_{Co} is the angle made by the magnetic moment M_{Co} of the Co sublattice with the c axis. The equilibrium direction of M_{Co} for a given applied field H is determined from the minimum of the free energy. The magnetic moments of the compound and the rare-earth ions are calculated as

$$M = -\frac{\partial F}{\partial H} = \sum_i M_R(i) + M_{Co}(T) \tag{5}$$

$$M_R(i) = -\sum_l \mu_B \langle i, l|L + 2S|i, l\rangle \frac{\exp[-E_l(i)/kT]}{Z(i)}. \tag{6}$$

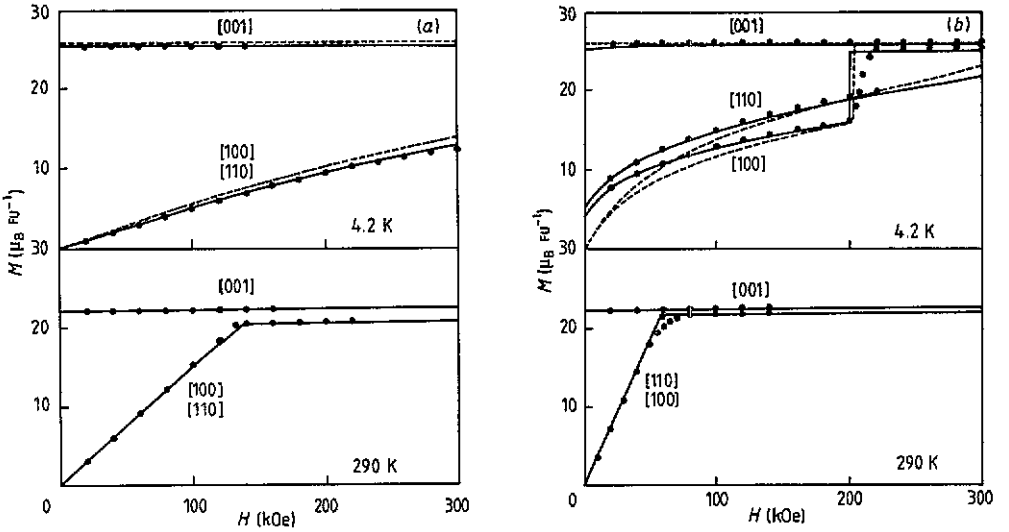

Figure 1. The magnetization curves of (*a*) $Pr_2Co_{14}B$ and (*b*) $Nd_2Co_{14}B$ along the [100], [110] and [001] axes at 4.2 and 290 K: ———, calculation in the space consisting of the ground and the first excited J multiplets; – – –, calculation in the space of the ground J multiplet; ●, experimental data [11].

It is assumed that $H_{ex}(T)$ is proportional to $M_{Co}(T)$. $M_{Co}(T)$ and $K_{Co}(T)$ are assumed to follow the temperature dependences of the $La_2Co_{14}B$ compound after scaling the different Curie temperature [7]. The value of $M_{Co}(0)$ is taken to be 19.4 μ_B and 19.6 μ_B per formula unit (FU) for $Pr_2Co_{14}B$ and $Nd_2Co_{14}B$, respectively, and the value of $K_{Co}(0) = -21.3$ K FU^{-1} is the same for $La_2Co_{14}B$ [7]. It is assumed, as has been observed for $R_2Fe_{14}B$ (R ≡ heavy rare earth) compounds [15], that the value of A_{nm} varies with the rare earth in proportion to $\langle r^n \rangle$, the average of nth power of the 4f-electron orbital radius, and the relation $|A_{22}|/A_{20} = 0.5$ holds as for the Gd compound [16]. A_{20} and A_{22} are assumed to vary with temperature in the same way. The higher-order CEF parameters are treated as invariant with temperature. Such a treatment would be reasonable since of all the CEF terms the A_{20} terms plays the major role in characterizing the magnetic properties, and the higher-order CEF terms become increasingly unimportant as the temperature rises. Our experience shows that a fully programmed fitting procedure based on the least-squares method does not give a satisfactory result, and our fitting procedure is characterized by adjustment of the values of the parameters through dialogue with the computer. The adjustment is guided by analysis of the role of each term in equation (1) in the magnetization [17–19].

3. Results and discussion

Figures 1 and 2 show the comparison of the calculations with experiments. Figures 1(*a*) and 1(*b*) show the magnetization curves along the [100], [110] and [001] axes at 4.2 and 290 K for $Pr_2Co_{14}B$ and $Nd_2Co_{14}B$, respectively. The magnetization curves at 4.2 K calculated within the ground J multiplet space are also shown for comparison. It can be seen that the neglect of the excited J multiplet apparently affects some of the $M(H)$

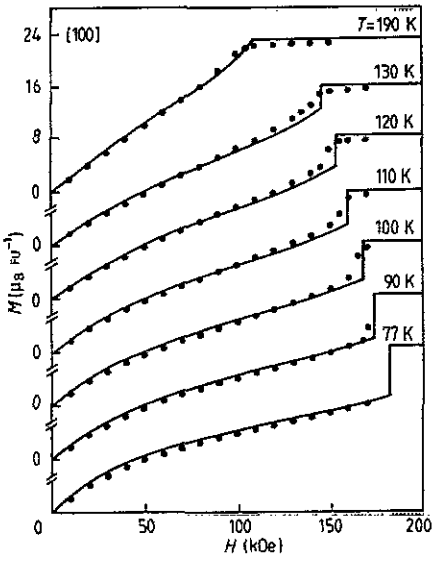

Figure 2. The magnetization curves of $Nd_2Co_{14}B$ along the [100] axis at a series of temperatures between 77 and 190 K: ———, calculation; ●, experimental data [9].

Table 1. The fitted values of $2\mu_B H_{ex}$ and A_{nm} at 0 K for $Pr_2Co_{14}B$ and $Nd_2Co_{14}B$.

	$Pr_2Co_{14}B$		$Nd_2Co_{14}B$		
	This work	Kato *et al* [11]	This work	Li *et al* [12]	Kato *et al* [11]
$2\mu_B H_{ex}$ (K)	+480	+440	+440	+410	+370
A_{20} (K)	+890	+980	+820	+780	+900
A_{22}/i (K)	±450	±380	±410	±410	±340
A_{40} (K)	+430	−170	+360	+80	−150
A_{42}/i (K)	0	0	0	0	0
A_{44} (K)	−220	0	−190	0	0
A_{60} (K)	−560	−1700	−460	−420	−260
A_{62}/i (K)	∓170	±120	∓140	0	±90
A_{64} (K)	−490	−900	−410	−390	−650
A_{66}/i (K)	±330	±350	±270	0	±310

curves, as has been pointed out in [15]. Figure 2 shows the magnetization curves of $Nd_2Co_{14}B$ along the [100] axis at a series of temperatures between 77 and 190 K. The calculated SR temperatures for the Pr and Nd compounds coincide with the experiments.

Table 1 lists the fitted values of $2\mu_B H_{ex}$ and A_{nm} at 0 K. The results of Li *et al* [12] and Kato *et al* [11] are also listed for reference. It should be noted that the sign of A_{40} for the $R_2Co_{14}B$ compounds is opposite to that for the $R_2Fe_{14}B$ compounds [15, 19–21]. The uncertainty of each parameter can be seen from the following data on the Nd compound, which demonstrate the variation in the calculation of the most sensitively affected quantity when the value of each parameter is changed separately. A decrease in the value of H_{ex} by 10% from that in table 1 increases the values of $M(H = 100\,\text{kOe})$ along the [100] and [110] axes at 0 K from 12.59 μ_B to 12.91 μ_B FU^{-1} and from 14.77 μ_B to 14.99 μ_B FU^{-1}, respectively. Increases in A_{20} and A_{40} and decreases in $|A_{60}|$, all by 5%, decrease the cone angle made by the EMD with the c axis at 0 K from 11.4° to 8.2°, 9.2°

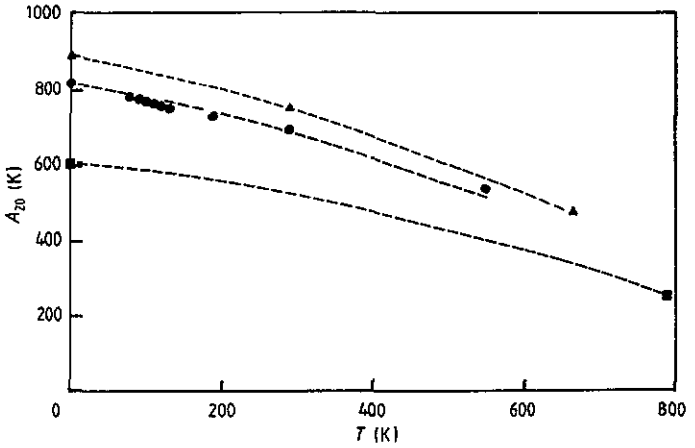

Figure 3. The temperature dependence of A_{20} for $Pr_2Co_{14}B$ (▲), $Nd_2Co_{14}B$ (●) and $Tb_2Co_{14}B$ (■).

and 5.4°, respectively. The variation in A_{42}/i ($\mathrm{i} = \sqrt{-1}$) from 0 to ∓ 140 K decreases and increases $M(H = 100\,\mathrm{kOe})$ along the [100] and [110] axes at 0 K from 12.59 μ_B to 12.34 $\mu_B\,\mathrm{FU}^{-1}$ and from 14.77 μ_B to 14.78 $\mu_B\,\mathrm{FU}^{-1}$, respectively. The variation on A_{62}/i from ∓ 140 to 0 K lowers $M(H = 100\,\mathrm{kOe})$ along the [100] and [110] axes at 0 K from 12.59 μ_B to 12.36 $\mu_B\,\mathrm{FU}^{-1}$ and from 14.77 μ_B to 14.30 $\mu_B\,\mathrm{FU}^{-1}$, respectively. The variation in A_{44} from -190 to 0 K makes the anisotropic field H_a along the [100] axis at 290 K lower than that along the [110], i.e. H_a along the [100] and [110] axes decreases from 56.9 to 54.0 kOe and from 56.8 to 56.6 kOe, respectively. The decrease in $|A_{64}|$ of 20% increases and decreases $M(H = 100\,\mathrm{kOe})$ along the [100] and [110] axes at 0 K from 12.59 μ_B to 12.68 $\mu_B\,\mathrm{FU}^{-1}$ and from 14.77 μ_B to 14.54 $\mu_B\,\mathrm{FU}^{-1}$, respectively. The decrease in $|A_{66}|$ of 20% increases the critical field of FOMP along the [100] axis at 0 K by about 5 kOe.

Figure 3 shows the variation in A_{20} with temperature for $Pr_2Co_{14}B$ and $Nd_2Co_{14}B$. The variation in A_{20} with temperature for $Tb_2Co_{14}B$ is also examined roughly as follows. The values of A_{nm} for $Tb_2Co_{14}B$ at 0 K are estimated from the relation $A_{nm}(\mathrm{Tb}) = A_{nm}(\mathrm{Nd})\langle r^n\rangle_{\mathrm{Tb}}/\langle r^n\rangle_{\mathrm{Nd}}$, and the value of $2\mu_B H_{ex}$ (=200 K) is estimated by extrapolating the values for the Pr, Nd and Gd compounds. The value for $Gd_2Co_{14}B$ ($2\mu_B H_{ex} =$ 220 K) is evaluated from its $M_s(T)$ curve [7]. The value of A_{20} at $T_{SR} = 790$ K is obtained by fitting the T_{SR}. As shown in figure 3, A_{20} for $Tb_2Co_{14}B$ also varies in a similar way to A_{20} for $Pr_2Co_{14}B$ and $Nd_2Co_{14}B$. A similar temperature dependence of A_{20} is also found for $NdCo_5$ and $SmCo_5$; detailed results will be reported elsewhere [22]. The origin of the temperature dependence of A_{20} is not clear.

The magnetization processes are analysed by using the fitted parameters as follows. Figures 4(*a*) and 4(*b*) show the free-energy difference $\Delta F = F(\theta_{Co}, \varphi_{Co}) - F(0, 0)$ as a function of θ_{Co} for $Pr_2Co_{14}B$ at a series of applied fields along the [100] ($\varphi_{Co} = 0$) and [110] ($\varphi_{Co} = 45°$) axis at 4.2 K, respectively. Figures 5(*a*) and 5(*b*) show the corresponding curves for $Nd_2Co_{14}B$. For $Pr_2Co_{14}B$, each curve has only one minimum, which moves towards larger θ_{Co} progressively with increase in H. No FOMP occurs at least up to 400 kOe, which coincides with experiment [11]. The behaviour of $Nd_2Co_{14}B$ along the [110] axis is similar. For this compound along the [100] axis, on the other hand, each curve has two minima. With increase in H, the equilibrium θ_{Co} corresponding to

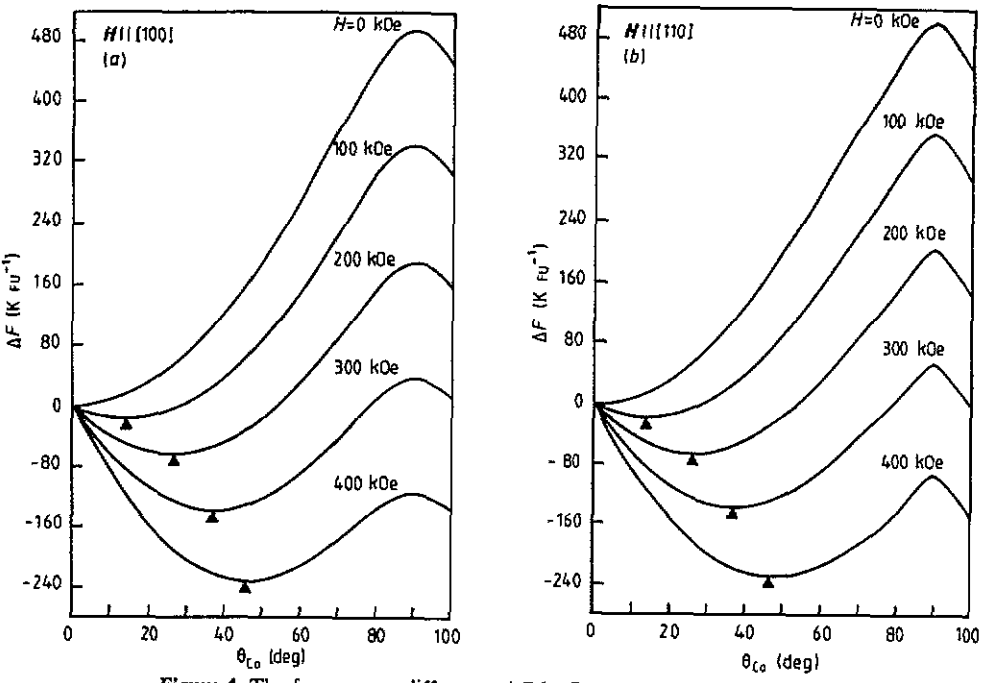

Figure 4. The free-energy difference ΔF for $Pr_2Co_{14}B$ as a function of θ_{Co} at a series of H applied along the (*a*) [100] and (*b*) [110] axes: ▲, lowest energy.

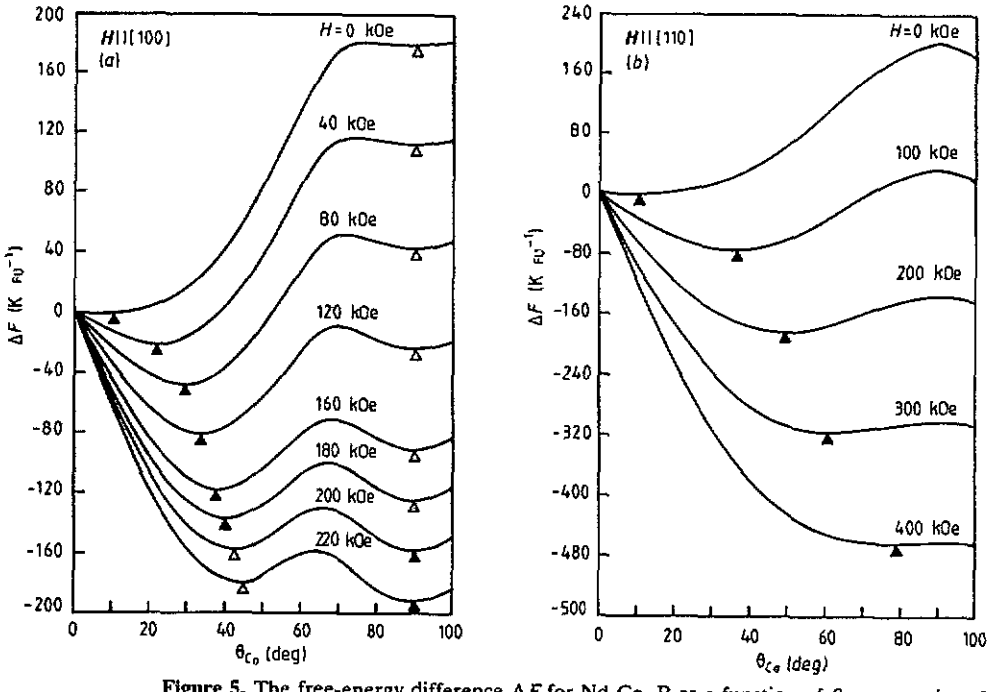

Figure 5. The free-energy difference ΔF for $Nd_2Co_{14}B$ as a function of θ_{Co} at a series of H applied along the (*a*) [100] and (*b*) [110] axes: Δ, higher minimum energy; ▲, lower minimum energy.

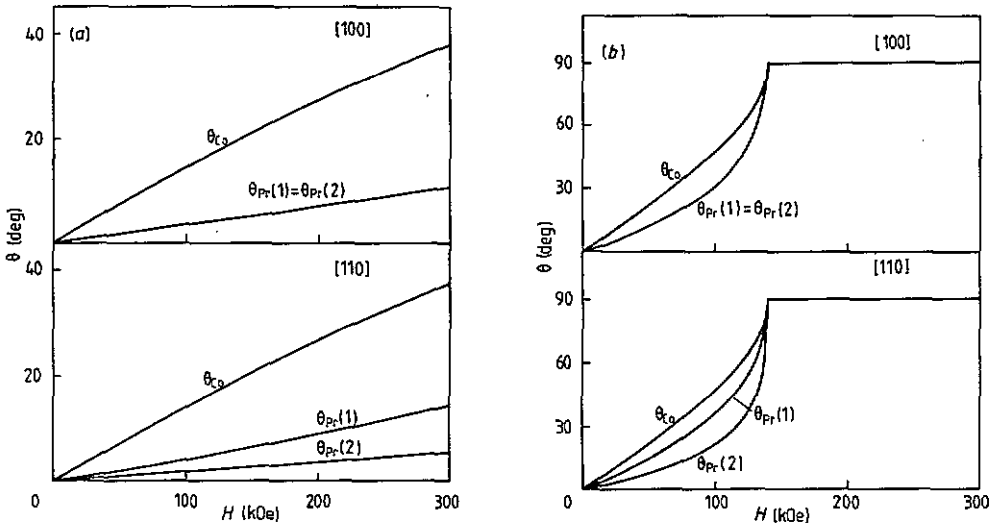

Figure 6. The field dependences of the angles θ_{Co}, $\theta_{Pr(1)}$ and $\theta_{Pr(2)}$ during the magnetization processes along the [100] and [110] axes at (*a*) 4.2 K and (*b*) 290 K for $Pr_2Co_{14}B$.

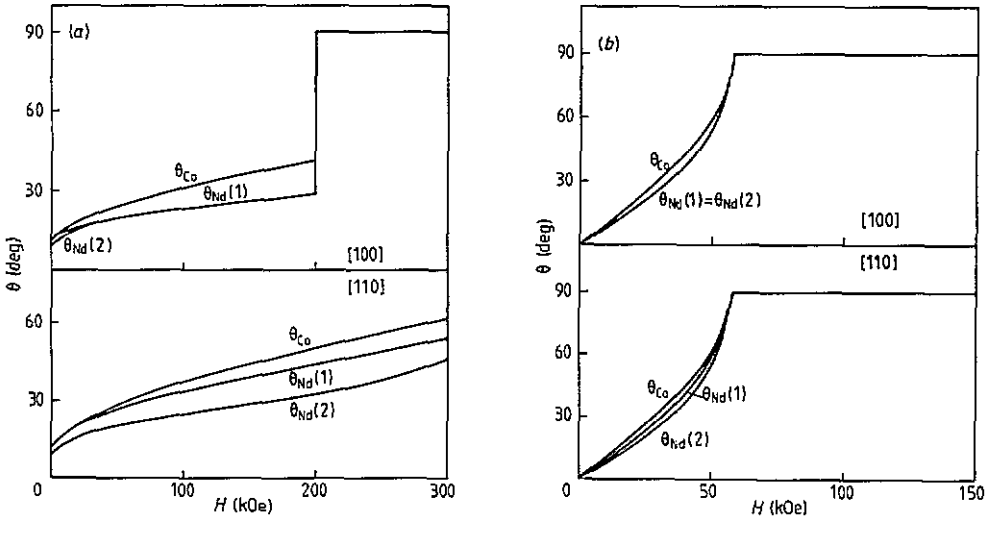

Figure 7. The field dependences of the angles θ_{Co}, $\theta_{Nd(1)}$ and $\theta_{Nd(2)}$ during the magnetization processes along the [100] and [110] axes at (*a*) 4.2 K and (*b*) 290 K for $Nd_2Co_{14}B$.

the lowest energy increases from 11.5° to 41.9° progressively and then jumps to 90° at 200 kOe. At this field, the new domain with $\theta_{Co} = 90°$ nucleates and grows through domain wall movement, which characterizes the FOMP. Figures 6(*a*) and 6(*b*) show the field dependences of the angles θ_{Co}, $\theta_{R(1)}$ and $\theta_{R(2)}$, made by $\boldsymbol{M}_{Co}$, $\boldsymbol{M}_{R(1)}$ and $\boldsymbol{M}_{R(2)}$ with the *c* axis, respectively, during the magnetization processes along the [100] and [110] axes for $Pr_2Co_{14}B$ at 4.2 K and 290 K, respectively. Figures 7(*a*) and 7(*b*) show the corresponding curves for $Nd_2Co_{14}B$. The non-collinearity between $\boldsymbol{M}_{Co}$ and $\boldsymbol{M}_R$ is more

striking for $Pr_2Co_{14}B$ than for $Nd_2Co_{14}B$; this is caused by the weaker R–Co exchange interaction and the stronger CEF interaction in the Pr compound.

Acknowledgments

This work was supported by the National Natural Science Foundation of China and partly by the Magnetism Laboratory, Institute of Physics, Chinese Academy of Sciences, Beijing, People's Republic of China.

References

[1] Buschow K H J, de Mooij D B, Sinnema S, Radwanski R J and Franse J J M 1985 *J. Magn. Magn. Mater.* **51** 221
[2] Le Roux D, Vincent H, L'Heritier P and Fruchart R 1985 *J. Physique Coll.* **46** C6 243
[3] Pedziwiatr A T and Wallace W E 1986 *Solid State Commun.* **60** 653
[4] Huang M Q, Boltich E B, Wallace W E and Oswald E 1986 *J. Magn. Magn. Mater.* **60** 270
[5] Pedziwiatr A T, Jiang S Y, Wallace W E, Burzo E and Pop V 1987 *J. Magn. Magn. Mater.* **66** 69
[6] Yamauchi H, Yamamoto H, Hirosawa H and Sagawa M 1987 *J. Magn. Magn. Mater.* **70** 340
[7] Hirosawa S, Tokuhara K, Yamamoto H, Fujimura S and Sagawa M 1987 *J. Appl. Phys.* **61** 3571
[8] Hiroyoshi H, Yamada M, Saito N, Kato H, Nakagawa Y, Hirosawa S and Sagawa M 1987 *J. Magn. Magn. Mater.* **70** 337
[9] Hiroyoshi H, Yamada M, Nakagawa Y, Hiorosawa S and Sagawa M 1987 *Proc. Int. Symp. on Physics of Magnetic Materials (Sendai, 1987)* (Singapore: World Scientific) pp 41–44
[10] Zhang L Y, Pourarian F and Wallace W E 1988 *J. Magn. Magn. Mater.* **74** 101
[11] Kato H, Yamada M, Kido G, Nakagawa Y, Hirosawa S and Sagawa M 1988 *J. Physique Coll.* **49** C8 575
[12] Li H S, Gavigan J P, Cadogan J M, Givord D and Coey J M D 1988 *J. Magn. Magn. Mater.* 72 L241
[13] Rose M E 1957 *Elementary Theory of Angular Momentum* (New York: Interscience)
[14] Hufner S 1978 *Optical Spectra of Transparent Rare-earth Compounds* (London: Academic) p 34
[15] Zhao Tiesong, Jin Hanmin and Zhu Yong 1989 *J. Magn. Magn. Mater.* **79** 159
[16] Smit H H A, Thiel R C and Buschow K H J 1987 *Physica* B **145** 329
[17] Zhao Tiesong, Jin Hanmin and Zhu Cheng 1986 *Chinese Phys. Lett.* 3 485
[18] Zhao Tiesong and Jin Hanmin 1987 *Solid State Commun* **64** 103
[19] Yamada M, Kato H, Yamamoto H and Nakagawa Y 1988 *Phys. Rev.* B **38** 620
[20] Givord D, Li H S, Cadogan J M, Coey J M D, Gavigan J P, Yamada O, Maruyama H, Sagawa M and Hirosawa S 1988 *J. Appl. Phys.* **63** 3713
[21] Cadogan J M, Gavigan J P, Givord D and Li H S 1988 *J. Phys. F: Met. Phys.* **18** 779
[22] Zhao Tiesong, Jin Hanmin, Guo Guanghua, Han Xiufeng and Chen Hong 1990 *Phys. Rev.* B at press